paper draft: supersat

K. Latimer

Jan 13, 2020

0 Outline

1. Introduction
2. Based on WRF simulations, under what conditions is quasi-steady-state (QSS) approximation for supersaturation (SS) valid? [A: need to specify stringent enough LWC and vert wind vel cutoffs, only take points below freezing level, and include rain drops and ventilation corrections]
3. Under above determined conditions, how do SS_{QSS} distributions from WRF compare to those from experiments (CAIPEEX, HALO)? [A: statistically significant differences in distributions]
4. Which variable contributes the most to the difference in SS_{QSS} distributions? [A: mean raduis and number concentration of water drops]
5. Do environmental conditions allow for a fair comparison between simulation and experiment in these cases? [A: it seems that aerosol PSDs are quite different in field campaigns than simulations, with higher overall number concentrations in the former cases. This calls into question the validity of directly comparing SS distributions.]

1 Introduction

introductory notes / lit review

2 Validity of QSS approximation for SS

- brief statement of quasi steady state formula
- we see agreement between actual and QSS supersaturation under the conditions (see fig 1):
  - T >273K (we're not including ice in the theory)
  - w >2 m/s (reasonably strong updrafts)

  - cloud LWC >1e-4 g/g (in the convection core)
  - including rain droplets and ventillation corrections

- upon applying above filters, the distribution of SS_{QSS} is shown in fig 2.

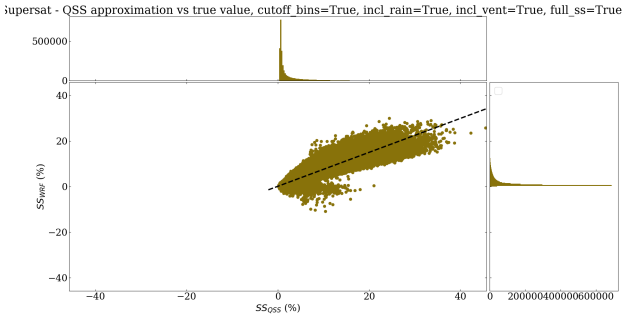

(a) Unpolluted case.

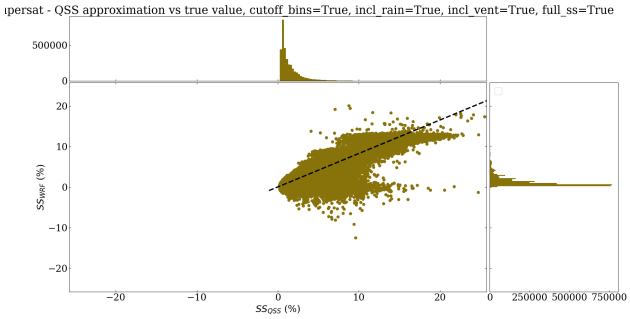

(b) Polluted case.

Figure 1: Actual (SS_{WRF}) vs predicted (SS_{QSS}) supersaturation. Histograms show the density of points along each axis.

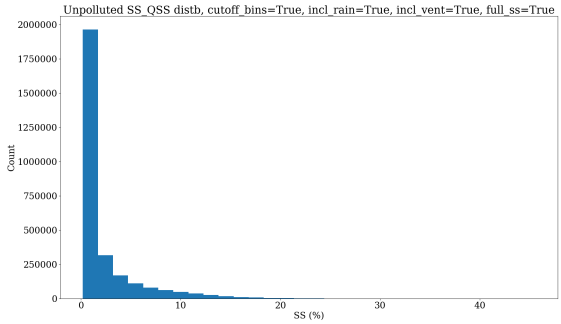

(a) Unpolluted case.

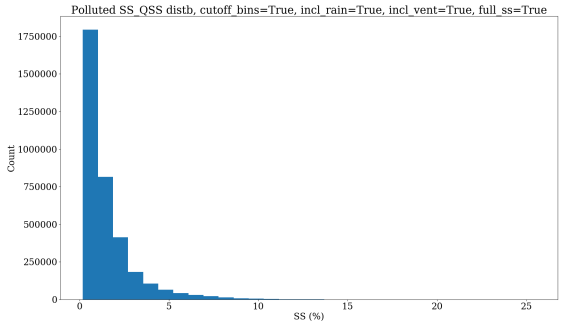

(b) Polluted case.

Figure 2: SS_{WRF} distribution in WRF simulation using filtering criteria described in the text.

3 SS_{QSS} distributions - simulation vs experiment

3.1 Distributions from field campaigns

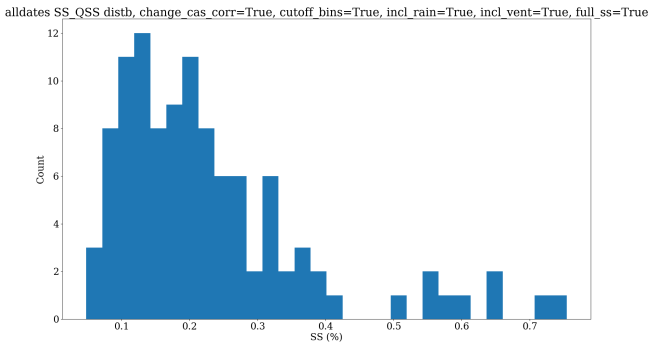

Figure 3: Predicted (SS_{QSS}) supersaturation distribution from HALO field campaign (all flight dates). Using filtering criteria outlined in section 2.

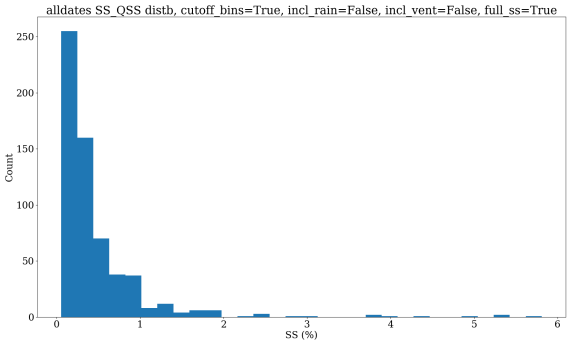

Figure 4: Predicted (SS_{QSS}) supersaturation distribution from CAIPEEX field campaign (all flight dates). Using filtering criteria outlined in section 2, but not including rain drops or ventilation corrections due to lack of data.

3.2 Statistical analysis of supersaturation distributions

3.2.1 Null hypothesis

Quasi-steady-state supersaturation values at selected sample of points from field campaigns are drawn from a "true" distribution like one of the ones from WRF.

3.2.2 Test

Reduced chi-squared

3.2.3 Details

Since altitude shows non-negligible correlation with SS_{QSS} in WRF data (Figure 5), we actually need to compare the experimental SS_{QSS} distribution to an adjusted simulated distribution, to account for the differences in altitude distributions for sampled points in both datasets. Specifically:

$$\tilde{\chi}^2 = \frac{1}{d}\Big(\sum_k \frac{(\mathcal{O}_k - E_k)^2}{E_k}\Big), \tag{1}$$

where k labels discrete bins into which we group supersaturation values and,

$\mathcal{O}_k =$ of measurements observed in bin k (for all flight dates combined)
$E_k =$ of measurements observed in bin k (under adjusted SS_{QSS} distribution $P'_{sim}(SS_k)$)

The adjusted distribution is given by:

$$P'_{sim}(SS_k) = \sum_j P'_{sim}(z_j, SS_k), \tag{2}$$

where,

$$P'_{sim}(z_j, SS_k) = \sum_{k''} \frac{P_{exp}(z_j, SS_{k''}) P_{sim}(z_j, SS_k)}{\sum_{k'} P_{sim}(z_j, SS_{k'})} \tag{3}$$

In this analysis, we had to use unequal bin sizes (i.e., group bins in the tail of the SS_{QSS} distributions) in order to ensure $E'_k \geq 5$ and $n_{SS\,bins} \geq 4$ (the standard criteria for this statistical test). We set $d = n_{SS\,bins} - 2$ to account for the two choices of number of bins in the bivariate probability distributions $P(z_j, SS_k)$.

NOTE for now comparing CAIPEEX distributions to those from WRF output excluding rain drops since we don't have that data from CAIPEEX yet. Applies to all statistical analyses following.

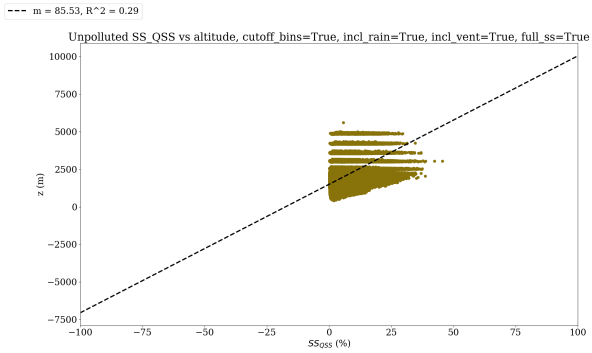

(a) Unpolluted case.

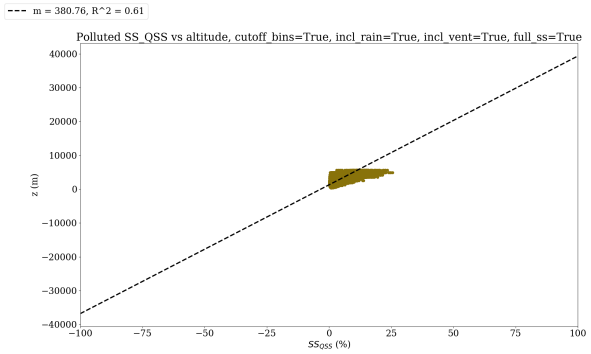

(b) Polluted case.

Figure 5: Scatter plots showing correlation between supersaturation as calculated in the QSS approximation and altitude in WRF simulations.

3.2.4 Results

WRF case	Num SS bins	Num z bins	$\tilde{\chi}^2_{HALO}$	$\tilde{\chi}^2_{CAIPEEX}$	$\tilde{\chi}^2_{0.990}$
Polluted	11	10	38.31	145.97	2.41
	11	20	48.39	155.30	2.41
	11	30	53.60	151.63	2.41
Unpolluted	11	10	46.03	139.21	2.41
	11	20	38.71	154.42	2.41
	11	30	71.07	163.77	2.41

Table 1: Reduced chi squared test statistics for comparison of experimental SS_{QSS} distributions to those in polluted and unpolluted cases of WRF simulation. Final column shows the critical value of $\tilde{\chi}^2$, above which we reject the null hypothesis at the 99% confidence level.

3.2.5 Comments

- For HALO: test statistics do show considerable sensitivity to binning arrangement, but are so far above the critical values that this seems largely irrelevant. We reject the null hypothesis in this case with very high (quantify?) certainty.
- For CAIPEEX: ditto. Chi-squared values are larger for this dataset because the sample size is higher (≈600 points cf ≈100 in HALO)

4 Causes of discrepancies between SS_{QSS} distributions (sim vs exp)

Up to temperature-dependent prefactors we have:

$$SS_{QSS} \sim \frac{w}{\langle f(r) \cdot r \rangle n}, \tag{4}$$

where w is vertical wind velocity, $f(r)$ is ventilation factor, r is water drop radius, n is water drop number concentration, and $\langle y(r) \rangle$ denotes the average of function y over the radial domain of the given drop size distribution. We compare the distributions of these three quantities in simulation vs experiment below in the same manner as for supersaturation in the previous section.

Overall, we find higher-valued test statistics for mean radius and number concentration distributions than for vertical wind velocity, suggesting that the drop size distributions rather than strength of vertical convection leads to the observed discrepancies in supersaturation distributions.

4.1 Mean radius (with ventilation correction)

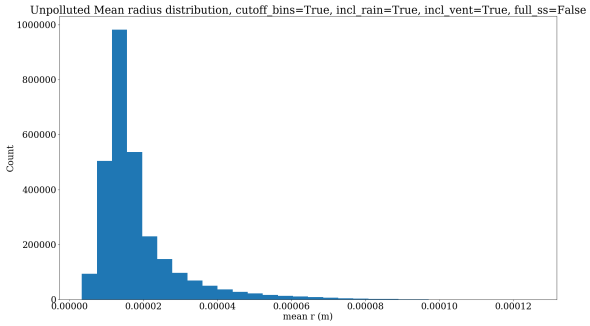

(a) Unpolluted case.

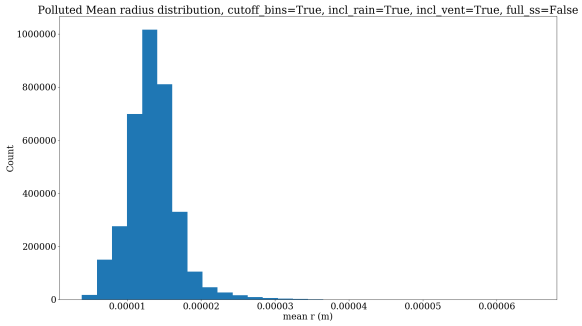

(b) Polluted case.

Figure 6: Mean radius (ventilation corrected) distribution in WRF simulation using filtering criteria described in the text.

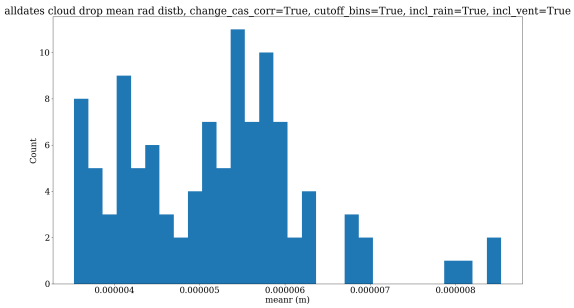

Figure 7: Mean radius (with ventilation corrections) distribution from HALO field campaign (all flight dates). Using filtering criteria outlined in section 2.

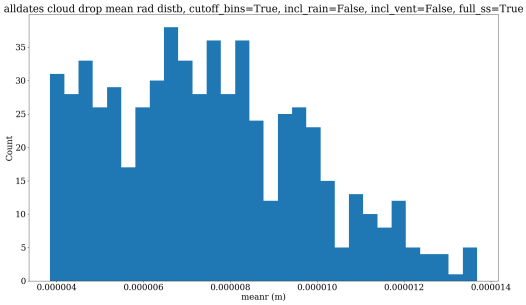

Figure 8: Mean radius distribution from CAIPEEX field campaign (all flight dates). Using filtering criteria outlined in section 2, but not including rain drops or ventilation corrections due to lack of data.

WRF case	**Num mean r bins**	**Num z bins**	$\tilde{\chi}^2_{HALO}$	$\tilde{\chi}^2_{CAIPEEX}$	$\tilde{\chi}^2_{0.990}$
Polluted	11	10	160.67	807.45	2.41
	11	20	216.59	808.90	2.41
	11	30	183.73	961.21	2.41
Unpolluted	11	10	118.23	908.96	2.41
	11	20	178.23	995.21	2.41
	11	30	128.76	803.49	2.41

Table 2: Reduced chi squared test statistics for comparison of experimental mean drop radius distributions to those in polluted and unpolluted cases of WRF simulation. Final column shows the critical value of $\tilde{\chi}^2$, above which we reject the null hypothesis at the 99% confidence level.

4.2 Number concentration

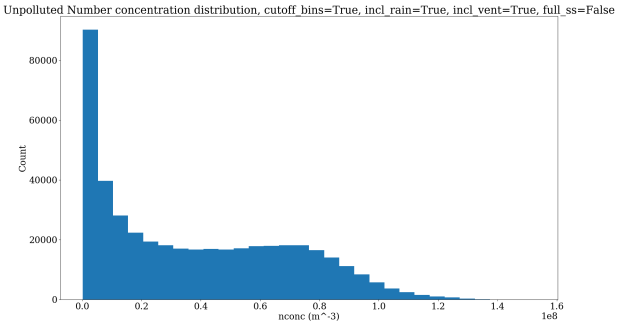

(a) Unpolluted case.

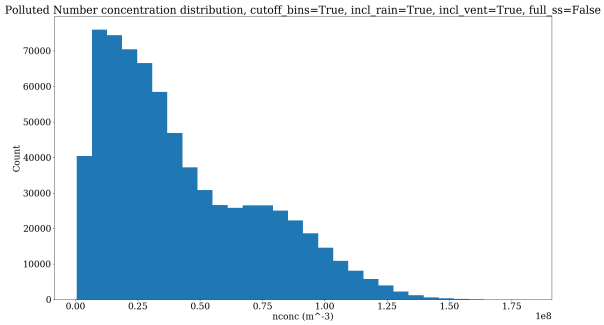

(b) Polluted case.

Figure 9: Number concentration distribution in WRF simulation using filtering criteria described in the text.

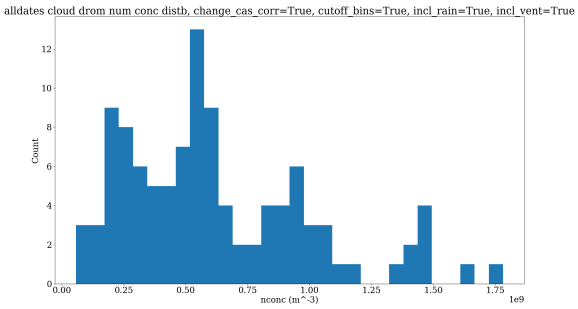

Figure 10: Number concentration distribution from HALO field campaign (all flight dates). Using filtering criteria outlined in section 2.

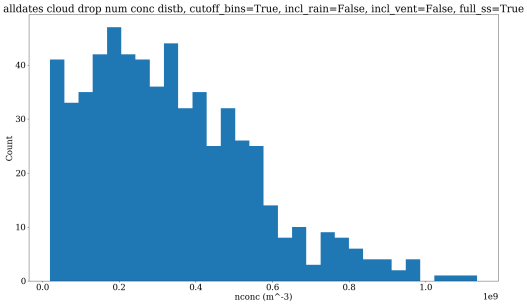

Figure 11: Number concentration distribution from CAIPEEX field campaign (all flight dates). Using filtering criteria outlined in section 2, but not including rain drops or ventilation corrections due to lack of data.

WRF case	**Num nconc bins**	**Num z bins**	$\tilde{\chi}^2_{HALO}$	$\tilde{\chi}^2_{CAIPEEX}$	$\tilde{\chi}^2_{0.990}$
Polluted	11	10	191.82	3446.05	2.41
	11	20	229.39	3397.21	2.41
	11	30	231.60	3564.48	2.41
Unpolluted	11	10	224.53	4344.51	2.41
	11	20	200.78	4450.17	2.41
	11	30	230.98	4685.65	2.41

Table 3: Reduced chi squared test statistics for comparison of experimental drop number concentration distributions to those in polluted and unpolluted cases of WRF simulation. Final column shows the critical value of $\tilde{\chi}^2$, above which we reject the null hypothesis at the 99% confidence level.

4.3 Vertical wind velocity

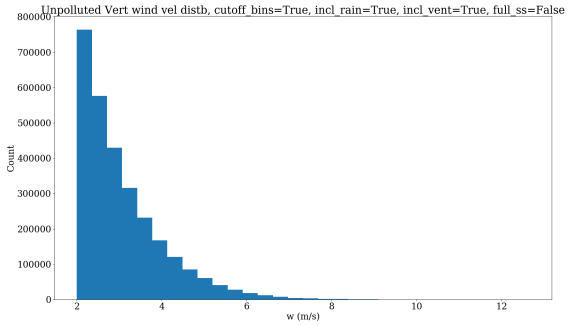

(a) Unpolluted case.

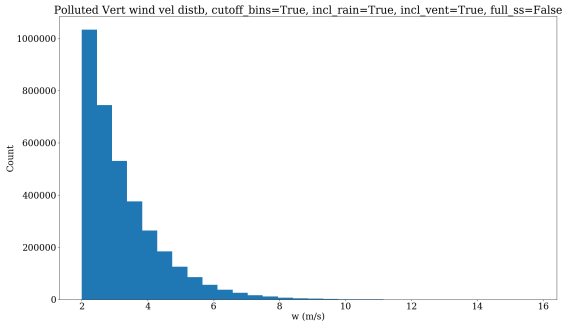

(b) Polluted case.

Figure 12: Vertical wind velocity distribution in WRF simulation using filtering criteria described in the text.

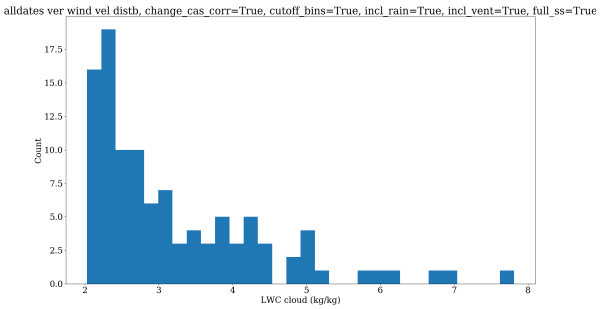

Figure 13: Vertical wind velocity distribution from HALO field campaign (all flight dates). Using filtering criteria outlined in section 2.

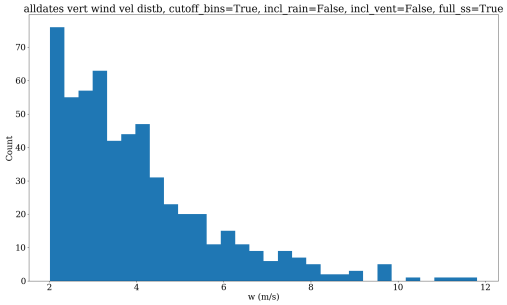

Figure 14: Vertical wind velocity distribution from CAIPEEX field campaign (all flight dates). Using filtering criteria outlined in section 2, but not including rain drops or ventilation corrections due to lack of data.

WRF case	**Num w bins**	**Num z bins**	$\tilde{\chi}^2_{HALO}$	$\tilde{\chi}^2_{CAIPEEX}$	$\tilde{\chi}^2_{0.990}$
Polluted	11	10	0.88	2.06	2.41
	11	20	0.96	4.19	2.41
	11	30	1.04	8.46	2.41
Unpolluted	11	10	1.68	51.34	2.41
	11	20	1.51	89.78	2.41
	11	30	1.16	87.23	2.41

Table 4: Reduced chi squared test statistics for comparison of experimental vertical wind velocity distributions to those in polluted and unpolluted cases of WRF simulation. Final column shows the critical value of $\tilde{\chi}^2$, above which we reject the null hypothesis at the 99% confidence level.

5 Environmental conditions - simulation vs experiment

5.1 LWC

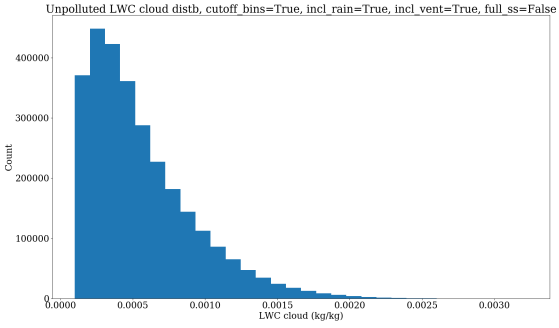

(a) Unpolluted case.

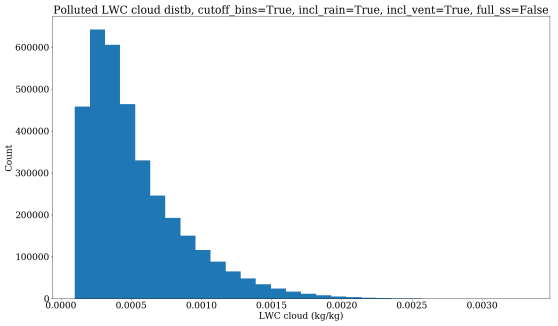

(b) Polluted case.

Figure 15: Cloud LWC distribution in WRF simulation using filtering criteria described in the text.

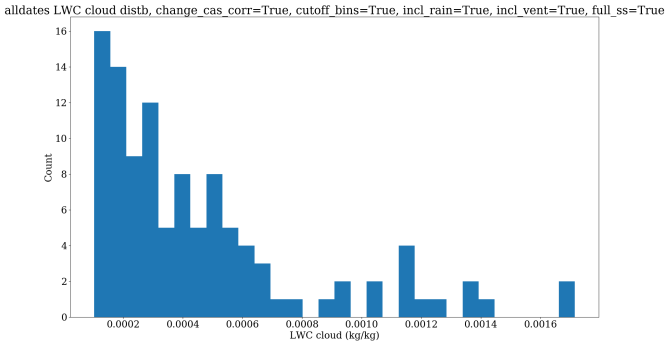

Figure 16: Cloud LWC distribution from HALO field campaign (all flight dates). Using filtering criteria outlined in section 2.

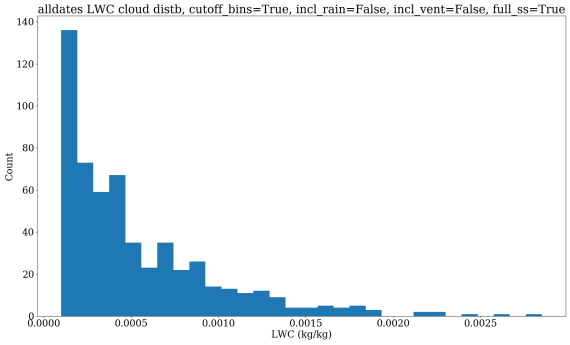

Figure 17: Cloud LWC distribution from CAIPEEX field campaign (all flight dates). Using filtering criteria outlined in section 2, but not including rain drops or ventilation corrections due to lack of data.

5.2 Aerosol PSD

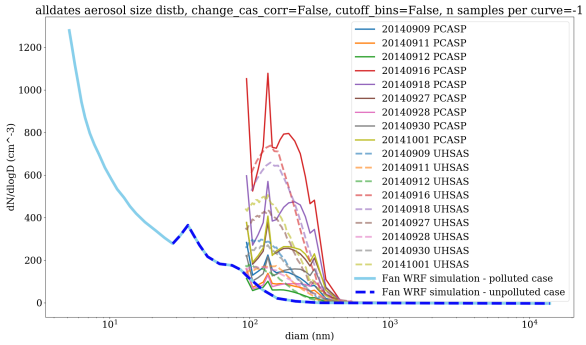

Figure 18: Aerosol particle size distribution from HALO field campaign (all flight dates), compared to initial distribution in boundary layer for WRF simulation. Using clear sky points (LWC 1e-5) below the freezing level.

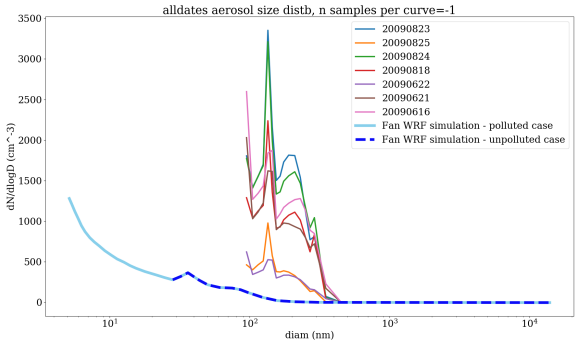

Figure 19: Aerosol particle size distribution from CAIPEEX field campaign (all flight dates), compared to initial distribution in boundary layer for WRF simulation. Using clear sky points (LWC 1e-5) below the freezing level.

6 Further discussion / conclusions

7 Figures to include in supplementary info

- all figures without lower bin cutoffs

- all figures without corrections from including raindrops / ventilation factors
- correlations between altitude and mean r, nconc, and w

8 TODO / remaining questions

- look at caipeex case study from 2011 w rain drop data available
- ditto for aerosol spectra at lower size ranges
- in code: optimize HALO instrument time offsets
- error analysis for experimental data
- look into commensurate binning in simulation / experiment comparisons?
- analytical justification for why actual and QSS supersaturation is still in linear relation
- expt vs model cloud/rain droplet size boundary

This is a reference [1].

References

[1] J. Fan, D. Rosenfeld, Y. Zhang, S. E. Giangrande, Z. Li, L. A. T. Machado, S. T. Martin, Y. Yang, J. Wang, P. Artaxo, H. M. J. Barbosa, R. C. Braga, J. M. Comstock, Z. Feng, W. Gao, H. B. Gomes, F. Mei, C. Pöhlker, M. L. Pöhlker, U. Pöschl, and R. A. F. de Souza, "Substantial convection and precipitation enhancements by ultrafine aerosol particles," *Science*, vol. 359, pp. 411–418, 1 2018.